Full Length Article

Hypergolic ignition induced by head-on collision of bi-propellant droplets: Monoethanolamine-based fuel and hydrogen peroxide

Dawei Zhang [a],[*],[1], Dehai Yu [b],[d],[*],[1], Yueming Yuan [b], Peng Zhang [c], Xuejun Fan [b]

[a] School of Mechanical Engineering and Rail Transit, Changzhou University, Changzhou 213164, China
[b] State Key Laboratory of High Temperature Gas Dynamics, Chinese Academy of Sciences, Beijing, China
[c] Department of Mechanical Engineering, City University of Hong Kong, Kowloon Tong, Hong Kong, China
[d] Department of Mechanics and Engineering Science, College of Engineering, Peking University, Beijing, China

ABSTRACT

Hypergolic ignition by the binary collision of H_2O_2 and Monoethanolamine (MEA)-$NaBH_4$ droplets has been experimentally studied with an emphasis on droplet inter-mixing, heat transfer, droplet swelling, and flame propagation. The entire ignition is phenomenally categorized into five stages. The H_2O_2 droplet penetrates the MEA-$NaBH_4$ droplet after the collision and coalesces with it. The H_2O_2 fluid rapidly restores its sphericity inside the coalesced droplet, which is theoretically proved to be driven by interfacial tension. The average measured restoration time is 14.0 ms. Large-scaled bubbles are generated at the interfacial structure, leading to swelling of the coalesced droplet. The existence of apparent interface tension tends to limit the rate of droplet inflation at the beginning. As more bubbles are produced, the interface tension wanes, and the droplet swells rapidly. The droplet surface expansion rate is identified via the gray-level information in recorded images. A theoretical model quantifying the swelling rate was established based on the underlying mechanism for the swelling of the reacting droplet, which can be attributed to the flash boiling of the superheated H_2O_2 fluid. As bubbles accumulate inside the coalesced droplet, a dual-bell-shaped droplet configuration is formed. A flame ring structure is observed when the ignition occurs. Luminant flame sustains more than 10 ms until the fuel vapor is depleted.

1. Introduction

Hypergolic bipropellants have been widely adopted in propulsion systems aiming at providing thrust and realizing maneuverability control [1–3]. Ignition of the hypergols takes place spontaneously once the fuel and oxidizer contact each other at the designed condition. It was evidenced in previous studies that the physical mixing between the propellants plays a crucial role in affecting the ignition process [1,4–9]. In a realistic propulsion system, the hypergolic propellants are brought into contact primarily in terms of droplet collision downstream of the injectors [10,11].

Issues about the structural characteristics of hypergolic ignition have been of interest for decades of years. Experimental attempts were made to disclose the ignition morphology under various circumstances. Among the works includes the investigation of hypergolic flame configuration by jet impingement [7,12,13]. Despite the insightful reported findings, it needs, however, finer spatial resolution for a detailed

structural illustration of the mixing between the hypergols. Other experiments [14–16] recorded the structure of the flame of the gelled propellants by employing the OH planar laser-induced fluorescence (PLIF). While laser-induced fluorescence requires the existence of corresponding radicals which unfortunately are not available for the pre-ignition stages. Due to the complexity of the ignition process and difficulties in experimental implementation, investigation on hypergolic ignition characters such as inter-mixing, heat transfer, and flame structure is still insufficient.

Distinct from the ignition and combustion of hydrocarbon droplets, which obtain energy from a hot environment or external heat source [17], for hypergolic ignition, the heat used to gasify the liquid-phased fuel and oxidizer is supplied from the heat released by exothermal reactions inside the droplet itself. The temperature inside the chamber at the engine-start condition is usually lower than that of the reacting droplets so the cold environment would herein play a role as a heat sink and might cause failure to the ignition [18]. Therefore, the prototype of inter-mixing and heat transfer between the bipropellant droplets

Nomenclature

B	impact parameter		Δ	droplet size ratio, $\Delta = D_F/D_O$
D	droplet diameter		γ	interfacial tension, $\gamma = \sigma_i - \sigma_o$
G	gray-level value		τ	scaled time
L	latent heat		Γ	correlated density $\Gamma = (\rho_o + \rho_i)/2$
l	wavenumber		β	droplet oscillation frequency
N	pixel number			
R	droplet radius		*Subscripts*	
T	temperature		b	boiling point
t	physical time		c	calculated value
U	the relative velocity between droplets		F	fuel (referred to as MEA mixture)
We	Weber number, $We = D_o U^2 \rho_O / \sigma_O$		i	the inner liquid
x	radial distance		m	experimentally measured value
α	thermal diffusivity		n	background average value
μ	dynamic viscosity		o	the outer liquid
ρ	density		od	oxidizer (referred to as H_2O_2)
σ	surface tension		r	referenced frame value
κ	droplet expanding rate		v	equilibrium vapor value
λ	thermal conductivity		∞	environmental value
			og	the original value of the merged drop

Table 1
Relevant physical properties (density, viscosity, surface tension, and boiling temperature) of H_2O_2, MEA, and $NaBH_4$ at room temperature.

	H_2O_2	MEA	$NaBH_4$
ρ(to water)	1.45	1.0	1.04
μ(mPa • s)	1.3	18.95	—
σ(mN/m)	80.4	49.0	—
T_b(K, 1 atm)	423	443	—

imposes an essential influence on the subsequent ignition event. The knowledge of the internal and external configuration of the reacting droplet is of great importance in revealing the mass and heat transfer patterns and in predicting the structure of the flame.

Comprehensive investigations on hypergolic ignition by droplet collision have been conducted by the authors via an experimental apparatus where a pair of freely moving fuel and oxidizer droplets can collide and mix under precise controls. Based on this experimental system, ignition of droplets of white fuming nitric acid (WFNA) and N,N, N′,N′- tetramethylethylenediamine (TMEDA) was firstly examined [19]. The dependences of ignition delay time on the collisional parameters, such as Weber number (*We*, ratio of inertial force to droplet surface tension), droplet size ratio (Δ), impact parameter (*B*, quantifying the degree of the off-center effect), and heat transfer related factor, droplet size (*D*), were systematically discussed [18,20]. Besides, the collision of the hypergolic droplets, under different dynamic conditions, was found featuring phenomenally in accordance with that by non-reactive drops, such as the collision of water or hydrocarbon droplets.

For mixing between hydrocarbon droplets, Tang et al [21] experimentally captured a 'jet-like' interaction pattern for unequal-sized droplets collision. The non-monotonic appearance of such 'jet-like' internal mixing with respect to *We* is found in line with the efficacy of *We* on the ignition delay time in our study [19]. Besides, previous studies [22,23] using non-hypergolic droplets have demonstrated that droplet separation is suppressed and hence droplet coalescence is promoted by increasing the size ratio due to the increasing viscous dissipation within the coalesced droplet. Unequal sized droplets collision not only inclines to produce more droplets coalescence but also promotes the interaction between the droplets.

Despite the phenomenal consistency of droplet collision with the ignition delay time, direct measurement of the intermixing within the

droplet during the pre-ignition stages is still undone. The reason for this deficiency mainly lies in the fact that the propellants, such as WFNA and TMEDA, for the most period of the ignition are severely veiled by a large amount of opaque vapor. The loss of droplet details makes it hardly possible to establish a quantitative interpretation of the inter-mixing and hence the flame formation. Moreover, as the ignition process itself involves intense exothermic chemical reactions, the droplets will be heated up and encounter phase transitions, e.g., liquid-phase propellants transformed into flammable gaseous species and nonflammable condensed-phase products. Such changes make the intermixing fashion more complicated than it appears in non-reactive droplet collisions.

The present study is following our previous works, with however the emphasis laying on a different topic: revealing the detailed inter-mixing and heat transfer patterns of hypergolic droplets during the preignition and specifying the flame structure and its propagation after ignition. To deal with the parameters one at a time, herein, we mainly concern the head-on droplet collisions (*B* = 0). The bi-propellant fuel and oxidizer are intendedly selected as the pair of the MEA-based fuel and the high-density hydrogen peroxide (H_2O_2) for the following reasons. First, as the saturated vapor pressure of MEA is much lower than that of the traditional ones such as WFNA and TMEDA, the dark vapor that blocks the droplet would be significantly suppressed. Second, the MEA takes on larger viscosity, which is quite prevalent a property among the hypergols, especially when referring to the gelled ones [24,25]. Characters of the ignition by the pair of MEA-base-fuel and H_2O_2 must therefore be of wide ubiquity for realistic usage. Finally, propellant H_2O_2 has been treated as one promising 'green' oxidizer and could provide comparable thrust [2,26–29]. Based on the above considerations, the present work is organized as follows. Experimental apparatus and instruction of the adopted hypergolic propellants are depicted in Section 2. Experimental observations and theoretical analysis about the droplet and flame pre- and after-ignition are presented in Section 3, followed by the concluding remarks.

2. Experimental setup and materials

2.1. Construction of hypergolic propellants

As depicted above, the pair of bipropellants utilized in the present study consists of H_2O_2 serving as the oxidizer and MEA as the liquid fuel. As a recipe, particles of sodium borohydride ($NaBH_4$) with superb reducibility [30,31], serving as activators, are initially dissolved in MEA
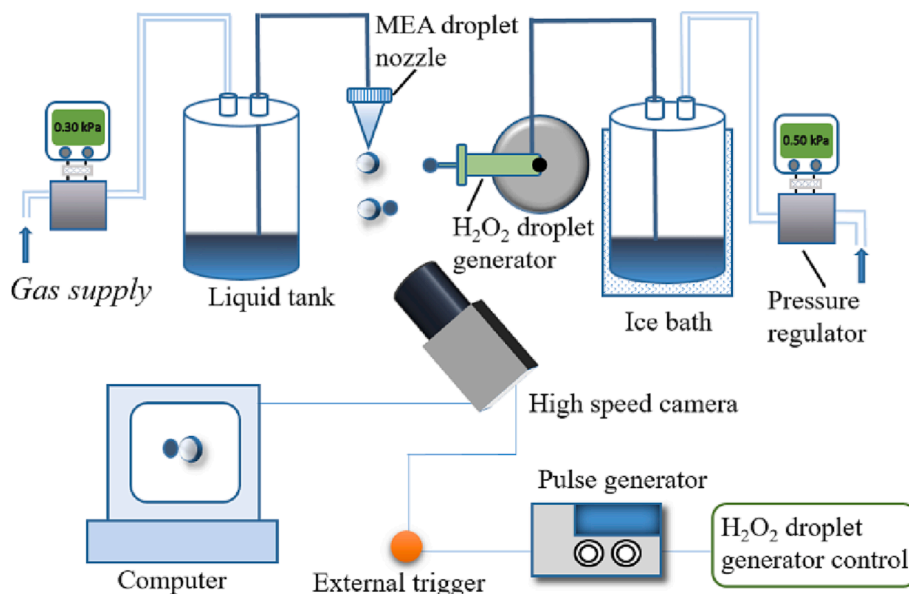
Fig. 1. Schematic of experimental apparatus employed for hypergolic ignition by a collision of H_2O_2 and MEA-NaBH$_4$ mixture droplets including droplet generation sub-system, dispensing regulation sub-system, and measurement system.
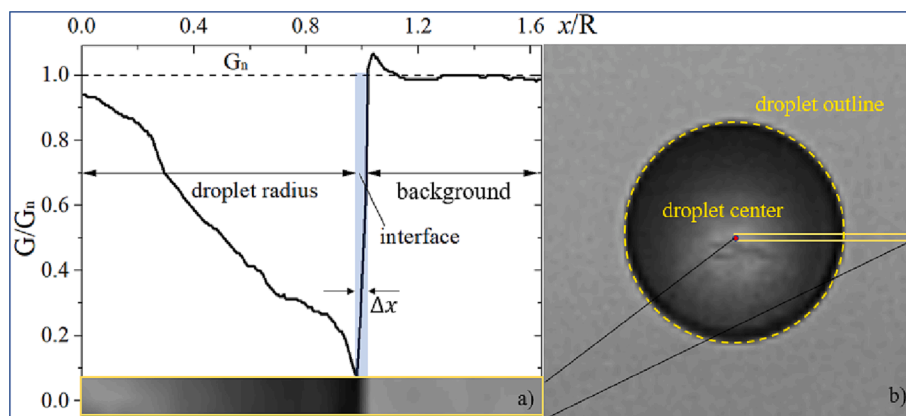

Fig. 2. Identification of droplet configuration using gray-level value (G) on intensity image: a) the calculated (G) as a function of radial distance; b) shadow image of a measured droplet.

liquid. As a result, when fuel mix with the oxidizer the NaBH$_4$ will first react with H_2O_2 releasing a large amount of heat which will then be used to achieve the gas-phase ignition. Values of interested physical properties of the ingredients are shown in Table 1.

The H_2O_2 liquid adopted is as pure as 92 % by weight and the fuel mixture is composed of MEA, 91 % by weight, and NaBH$_4$, 9 % by weight. A fraction of 9 % as adopted in the present study is considered a guarantee for the hypergolicity at the operating condition since in the previous experiments of hypergolic ignition on drop tests, the fraction of NaBH$_4$ can reach as high as 7 % [29], which is a little lower than that in the present work. The NaBH$_4$ particles were added into the fuel liquid via a set of ultrasonic stirrers operating in a desiccative environment to avoid the deliquescence of NaBH$_4$. The fuel mixture was placed in a desiccative environment for more than one week before the experiment to ensure that no sediments exist.

2.2. Description of the test rig

The binary collision of freely moving H_2O_2 and MEA-NaBH$_4$ fuel mixture droplets was realized by upgrading the experimental apparatus employed in our previous study [19]. As shown in Fig. 1, a set of

spatially fixed needle-shape nozzle is employed to generate fuel mixture droplets whose size depends primarily on the diameter of the nozzle orifice and secondarily on the liquid flow rate. Generation of H_2O_2 droplets was achieved through a set of the micro-electromagnetic nozzle from Fritz Gyger AG. To suppress the self-decomposition of H_2O_2, the liquid tank was maintained in an ice bath and the transport pipelines were under light-shading treatment throughout the experiments. The collision is regulated by precisely adjusting the set of the $XYZ-\alpha$ stage with a spatial resolution of 2 μm. The frequency of the collision and ignition event was intentionally controlled up to 3 Hz to avoid interference from the neighbor ones.

The initial pressure of the environment where the fuel and oxidizer droplet collide is just the ambient pressure and the operating pressure in the fuel and oxidizer tank is no more than 100 kPa to eject droplets. The initial temperatures of the fuel and oxidizer are the ambient temperature and ice point respectively.

2.3. Measurement methodology

For the measurement part, a set of high-speed-camera was utilized to record the entire ignition process with a capturing rate of 5000 fps
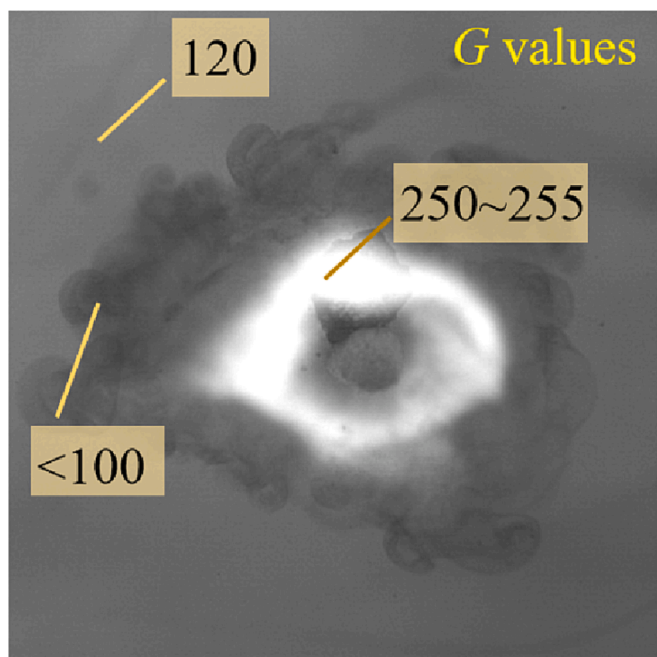
Fig. 3. Identification of dark vapors, background, and bright flame using G values: $G = 100$ for the background; G less than 100 for dark vapors; G greater than 250 for the bright flame.

(frames per second) and an exposure of 5 μs, a period that has been verified short enough to freeze droplet motion in an image. The size and speed of the original droplets, as well as the dark vapor and bright flame, were detected and measured via an analyzing program based on the information of the gray-level value (G) of each pixel in images. In specific, the droplet occupation area in the shadow image is recognized from the background (with an average gray level of G_n) by the large discrepancy in the level of darkness between them. Fig. 2a schematizes an image band extracted from a droplet image shown in Fig. 2b. Distribution of the normalized gray-level G/G_n in the function of distance × registers that there exists a narrow interface area, Δx, where G sharply increases from the minimum value that denotes the edge of the droplet to a relatively high level comparable to G_n (the value of G/G_n equals nearly to 1.0). The real edge of the droplet is located at some certain spot within Δx. In such a way, the error of identification of the configuration of the droplet, defined as $\Delta x/R$, can be calculated and has been verified by no more than 3 %. Note also that for the gray-level distribution across the droplet, G/G_n values near 0.7 at the droplet center and then decrease to the minimum at the droplet edge. The relative brightness at the central area is caused by the imaging of the backlight within the droplet.

The grayscale images of the shadow photographs are stored with a resolution of 8 bits per sample pixel, which results in 256 different grayscale levels for the shade of gray. The lowest level, 0, denotes the darkest, and the highest level, 255, is the brightest. With the average grayscale level set to 100, the grayscale levels that are less than 100 represent the dark gaseous species, and those higher than 250 (less than 255) in the region are considered luminous flames, as shown in Fig. 3. The accuracy of the selection of the threshold of grayscales is tested and verified in our previous study [19]. The uncertainty is less than 0.1 ms in identifying the occurrence of the flame.

In the present study, the collision Weber number is defined as $We = \rho_{od} U^2 D_{od}/\sigma_{od}$. The usage of the oxidizer's physical properties in We is for concise illustration and convenient calculation. The Weber number herein ranges from 20 to 100, which is within the value range of common interest for droplet collision in practical applications [11,23]. The value of We in the present work is regulated through the adjustment of droplet relative velocity which is controlled by the supplying gas

pressure. For droplet size ratio, it is evaluated as $\Delta = D_F/D_{od}$, viz., the ratio of the diameter of the fuel mixture droplet to the oxidizer droplet. The droplet size ratio ranges from 1.35 to 2.15 under two considerations. First, according to the collision dynamic results, binary droplets with unequal sizes would lead to more coalescence cases. Second, the inter-mixing between the two colliding droplets would be expedited especially when the smaller droplet impacts the larger one. Note that the size of the fuel mixture droplet is fixed in the experiment, while the oxidizer droplet size is changed as required.

3. Results and discussion

3.1. Five pre-ignition stages concerning droplet morphology

Analogous to the ignition of WFNA/TMEDA, the ignition induced by binary collisions of MEA-based fuel and H_2O_2 droplets is phenomenally divided into five stages. For clear illustration, a representative case at $We = 31$ and $\Delta = 1.75$ is selected and its ignition process is shown in Fig. 4. The length scale in each focusing frame, as indicated in corresponding images, is adjusted such that all details of the droplet, vapor and flame can be exhibited. All the pre- and after-ignition stages are presented chronologically under the same time scale of a millisecond. The main features in each stage are depicted in what follows:

Stage I: Droplet collision and deformation (0 ~ 20 ms). This stage starts from the moment when the two droplets are just about to collide. After impacting each other the droplets severely deform from the spherical shape. Nevertheless, the outline of the droplet remains sharp and clear. The interacting and deforming pattern of the droplets is quite similar to that of the non-reactive drops, indicating that the chemical reaction is negligible during Stage I.

Stage II: Occurrence and development of inter-mixing structure (20 ~ 42 ms). In this stage, the deformation and oscillation of the droplet have ceased. As shown in the images in the third row. the two bipropellant droplets now merge into a larger one that returns to the spherical shape. Although the droplet outline is still unaltered, the special structure can be recognized in the interior area. Particularly, an interfacial boundary restricting the internal structure can be discerned, as shown at 30.0 ms. The inner structure develops, becoming darker and darker as indicated from 40.0 ms to 42.0 ms.

Stage III: Droplet expansion. In course of the development of the inter-mixing structure within the droplet, at some certain moment, the droplet suddenly starts to expand characterized as the inflation of the volume. The expansion develops so fast that the droplet deforms again from being a sphere in a short period from 46.0 ms to 47.4 ms. Along with the inflation of the droplet, a visible amount of opaque vapor is detected, although it makes still no difference in capturing the internal structure and the configuration of the droplet.

Stage VI and V: Dual-bell droplet formation and ignition. As the droplet keeps inflating, it deforms further into a double-bell shape, as shown at 48.6 ms and 49.2 ms. The two spherical parts of the droplet connect by a waist structure and present themselves in observable distinction: the appearance of the upper sphere looks much brighter and more transparent than the lower one. When it goes to 50.0 ms, a ring-shaped flame surrounding the waist of the droplet emerges, signifying the beginning of the ignition. The luminous flame then expands outwardly at a rapid speed, enveloping the droplet within several milliseconds. The bright flame maintains for more than 15 ms afterward. The two parts of the droplet eventually separate away from each other leaving two inflammable products streaking through the bright flame zone, as seen from 57.0 ms ~ 65.0 ms.

From experimental observation, the opaque vapors block the reacting droplet during the pre-ignition stages, as what happened in the ignition of WFNA/TMEDA droplets, did not show up in the present case. The suppression of the dark vapors lets us succeed to capture and measure the detailed inter-mixing structures and the configuration of the subsequent flame.
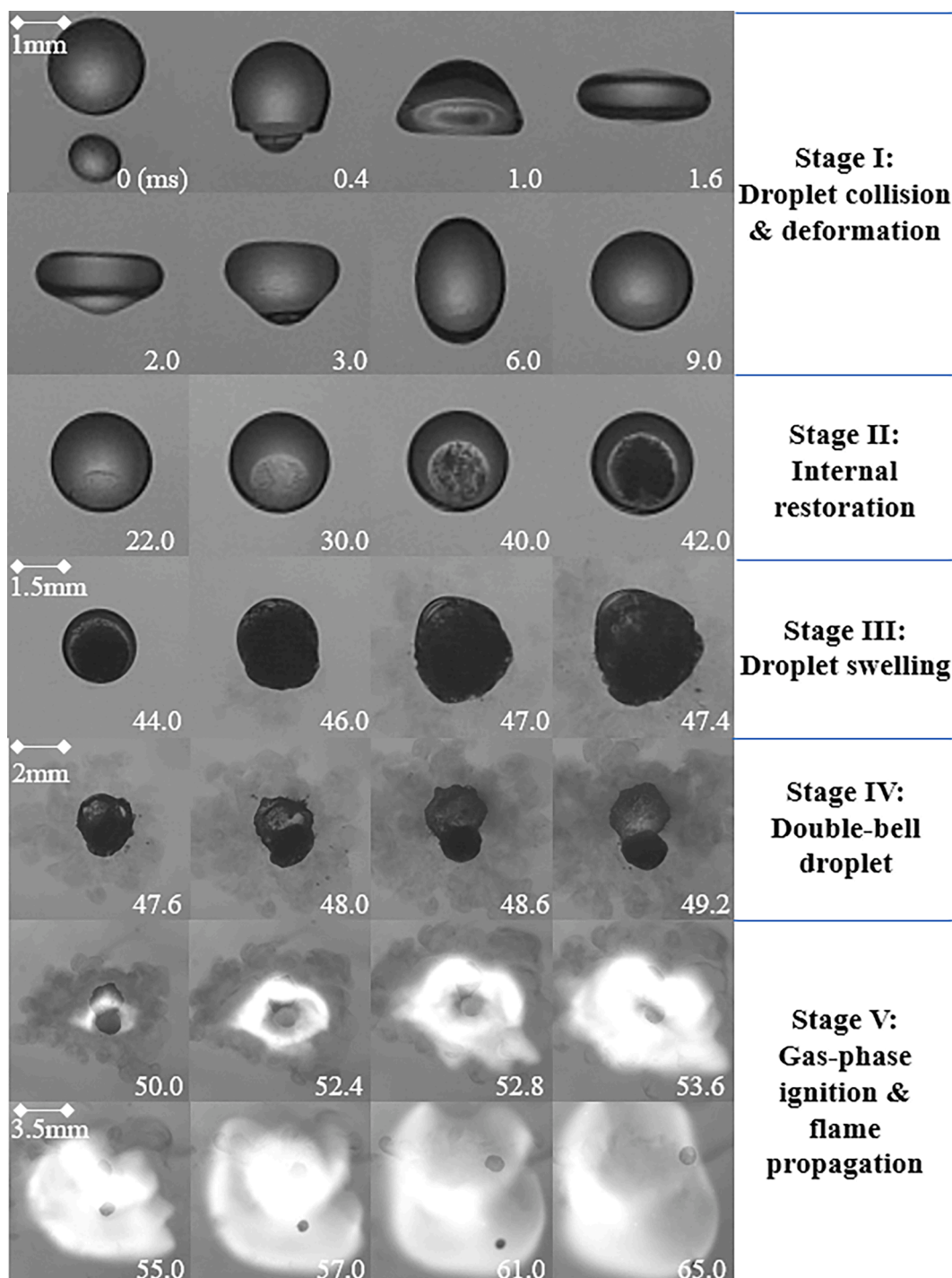
Fig. 4. Representative shadow images in the time sequence of hypergolic ignition process by H_2O_2 and MEA-NaBH$_4$ fuel mixture droplets collision at $We = 31$ and $\Delta = 1.75$.

3.2. Intermixing within the coalesced droplet

The origination of the inter-mixing structure inside the droplet, as observed in Stage II, can be traced back to the moment the oxidizer droplet impacted the fuel droplet. After coalescence, the smaller oxidizer droplet severely deforms inside the larger fuel droplet. Since at this stage, the chemical reaction rate is negligible yet, the observed growth of the internal structure can be soundly considered as the restoration of the deformed oxidizer mass.

A sharp interfacial line distinguishing the contour of the internal structure is employed to quantify the rebounding process. As shown in

Fig. 5, the boundary line initiates from a relatively flat shape at M_1 and then shifts to an arcuate one, which in turn changes to a circular shape, as seen from M_2 to M_3 and M_4. The ratio of curvature of the initial colliding oxidizer droplet to that of the interfacial boundary, $(1/R_{od})/(1/R) = R/R_{od}$, is plotted in function of physical time in Fig. 5. It is found that this ratio decreases abruptly from a relatively high value down to its minimum (approaching to 1.0). The decrease of $(1/R_{od})/(1/R)$ covers the entire rebounding process of the inner mass. Here we denote the radii of the flat-, arcuate-, and the restored spherical-interfacial-boundary by R_1, R_2, and R_3 respectively. From the figure, one can recognize that R_1 is remarkably larger than R_2 in accordance
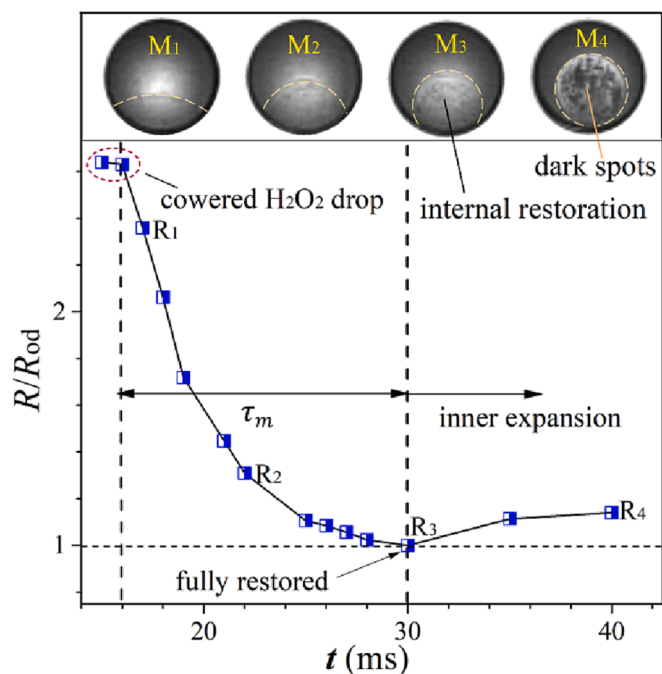
Fig. 5. Development of the internal structure from the flat shape at R₁, arcuate shape at R₂, spherical chape at R₃, and the light expanded shape at R₄, corresponding to the images at moments M₁ ~ M₄ respectively; the curvature ratio is plotted in function of time.
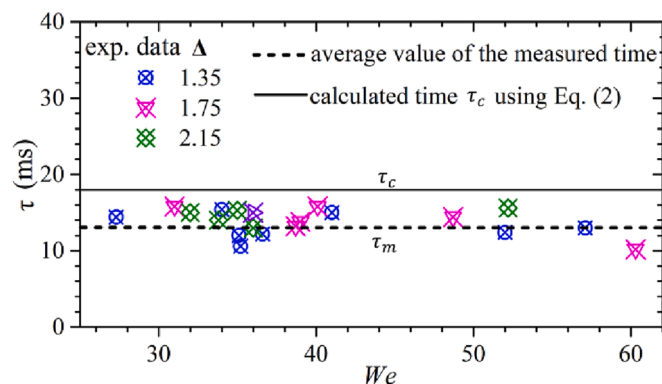

Fig. 6. Experimental data of the restoration time, τ, in the function of We at size ratios of 1.35, 1.75, and 2.15; the averaged measured time is τ_m and the calculated time is τ_c from Eq. (2).

with the shapes they represent. R_3 represents the minimum value of the curvature ratio, indicating that the rebounding process has been completed. The inner mass now retakes the size and shape of the droplet before the collision. The fully restored internal drop then starts to wriggle inside the fuel mixture droplet and expand in volume as the effective radius R_4 at 40 ms develops larger than R_0 (the ratio larger than 1.0).

For quantitative interpretation of the rebounding process, based on the development of the curvature of the internal boundary, we define a restoration time τm as the time interval from the beginning of the decrease of $(1/R_{od})/(1/R)$ (in the representative case referring to the moment of cowered H₂O₂ drop state) to the moment the droplet fully restores its shape (referred as to R_3). The rebounding time under the
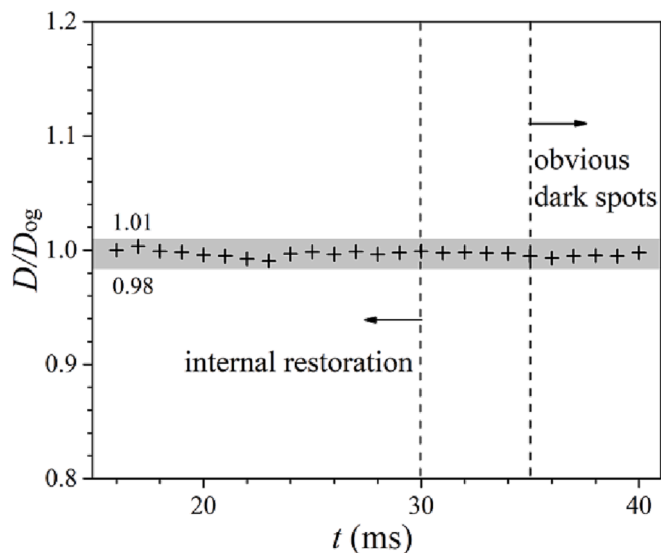

Fig. 7. Normalized droplet size during Stage II: covering the periods of internal restoration and the occurrence of the inner dark spots.
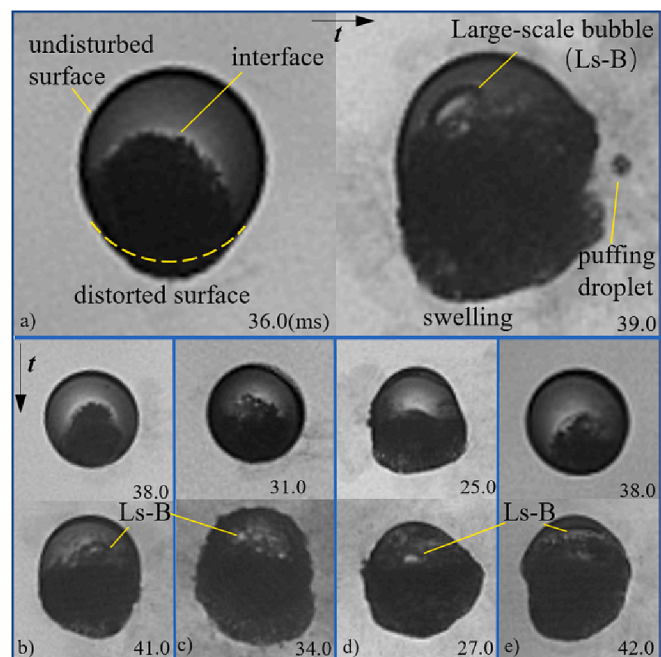

Fig. 8. Droplet swelling images at a)$We = 41$, $\Delta = 1.75$; b) $We = 61$, $\Delta = 1.75$; c)$We = 31$, $\Delta = 1.35$; d)$We = 61$, $\Delta = 1.35$; and e) $We = 41$, $\Delta = 2.15$.

such definition is with a value of 14.0 ms for the representative case. Restoration time for other cases is measured and shown in Fig. 6.

To reveal the underlying mechanism of the inner restoration, an *ad-hoc* theoretical model calculating the restoration time is constructed herein based on the linear instability analysis reported by Miller [32], quantifying the relaxation of a single droplet immersed in a viscous liquid environment. Droplet oscillation frequency, β, under such circumstances is expressed in terms of the wavenumber, l, and of the physical properties of the two relevant liquids by
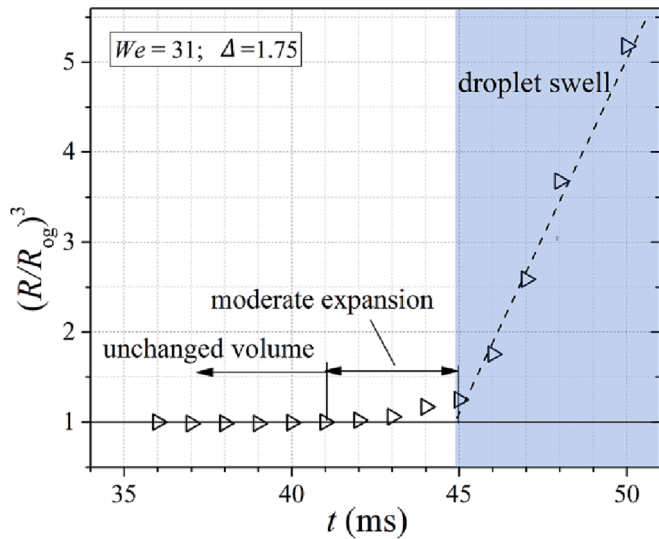
Fig. 9. Droplet swelling at $We = 31$, $\Delta = 1.75$, including unchanged volume, moderate expansion, and the rapid swelling periods; normalized droplet volume $(R/R_{og})^3$ is plotted in function of time.
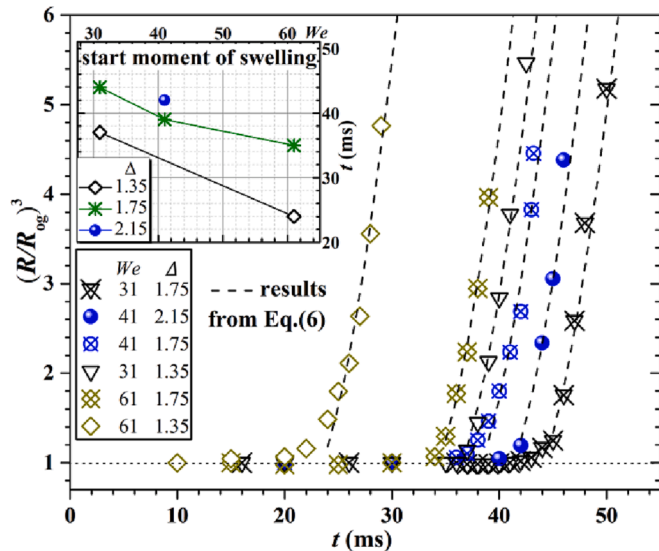

Fig. 10. Droplet swelling in terms of normalized volume $(R/R_{og})^3$ at various *We*s and Δs. Sub-figure presents starting moments of swelling. The dashed line is the theoretical prediction by Eq. (6).

$$\beta = \frac{(2l+1)^2 \sqrt{\beta^* \mu_i \mu_o \rho_i \rho_o}}{2\sqrt{2}R\Gamma[(\mu_i\rho_i)^{1/2} + (\mu_o\rho_o)^{1/2}]} + \frac{(2l+1)\left[2(l^2-1)\mu_i^2\rho_i + 2l(l+2)\mu_o^2\rho_o + \mu_i\mu_o(\rho_i(l+2) - \rho_o(l-1))\right]}{2R^2\Gamma\left(\sqrt{\mu_i\rho_i} + \sqrt{\mu_o\rho_o}\right)^2} \tag{1}$$

According to linear stability analysis, the oscillatory behavior of the droplet can be interpreted by the superposition of all available oscillating modes characterized by the wavenumber. Since the oscillating modes depend identically on the related physical quantities, e.g., density, viscosity, and dimensionality, we constructed the ad-hoc model by merely discarding the wavenumber-related information and appropri-

ately scaling these physical properties. The resultant formula for the calculated rebounding time (τ_c) was thus established as

$$\frac{1}{\tau_c} \quad \frac{\sqrt{\beta^* \mu_i \mu_o \rho_i \rho_o}}{R\Gamma\left(\sqrt{\mu_i\rho_i} + \sqrt{\mu_o\rho_o}\right)^2} + \frac{\mu_i^2\rho_i + \mu_o^2\rho_o + \mu_i\mu_o|\rho_i - \rho_o|}{R^2\Gamma\left(\sqrt{\mu_i\rho_i} + \sqrt{\mu_o\rho_o}\right)^2} \tag{2}$$

where $\Gamma = (\rho_o + \rho_i)/2$ is the correlated density, and $\beta^* = (\gamma/\Gamma R^3)^{1/2}$ is the frequency of droplet natural oscillation driven by interfacial tension. The interfacial tension herein is simplified by the model of $\gamma = \sigma_i - \sigma_o$ [33].

Fig. 6 shows the average restoration time τ_m from the experiment and the calculated time τ_c from Eq. (2) at various *We*s and Δ s. According to the experimental and the calculative results, the restoration of the droplet is insensitive to collision parameters such as *We* and Δ. The value of τ_m for all the collision cases is 13.0 ms which agrees well with the value of τ_c. Note that Eq. (2) is formulated under the mechanism that the interfacial tension acts as the driving force and thus the droplet colliding dynamical parameters such as *We* and Δ are absent in the equation. This can explain and prove: first, the internal restoration is independent of the colliding dynamical parameters; second, the rebounding process within the droplet should be impelled by the interfacial tension between the oxidizer and fuel mixture.

In addition to the shape change inside the droplet, in course of the internal expansion, one can observe a bunch of dark spots appearing at the surface of the restored internal structure, as shown at moment M_4 in Fig. 5. These dark spots are reasonably considered as the solid-phased sodium borate, the product of the redox reaction between NaBH$_4$ and H$_2$O$_2$. Nevertheless, although there appear solid products inside the droplet, the condensed phase reaction during this stage is considered still proceeding at a moderate rate because the merged droplet maintains its shape during the such stage. As indicated in Fig. 7, the ratio of the diameter of reacting droplet in Stage II to coalesced droplet size, D/D_{og}, evaluates within a narrow range of 0.98 ~ 1.01, denoting that coalesced mixture droplet keeps almost unchanged during the corresponding periods of internal restoration and occurrence of dark sports.

3.3. Droplet swelling with internal flash evaporation

The restored internal structure inside the merged droplet continues expanding as the exothermal liquid-phase reaction proceeds. Once the surface constraint was overwhelmed by the inner pressure, the droplet would start to swell. Fig. 8 schematizes the general features of the swelling process for various collision cases. In the beginning, the droplet expands at the polar zone where the oxidizer initially impacted and restored. The outline of the droplet at such an area starts to distort, as shown in Fig. 8a, and the corresponding hemispherical part turns solid-like due to the aggregation of the opaque products. While at the other polar part, the droplet outline remains intact-its surface looks the same and there are no chemical reactions ongoing. An interface separating the

distorted and the undisturbed parts can be identified inside the droplet.

Employing our image analysis program, the deformed occupation area of the droplet and its equivalent size can be identified. Fig. 9 shows for the representative case the development of the normalized droplet volume, R^3/R_{og}^3, where the referenced value R_{og} represents the merged droplet radius before swelling. The value of R^3/R_{og}^3 maintains a minimum at the value of 1 over the whole collision stage I and internal
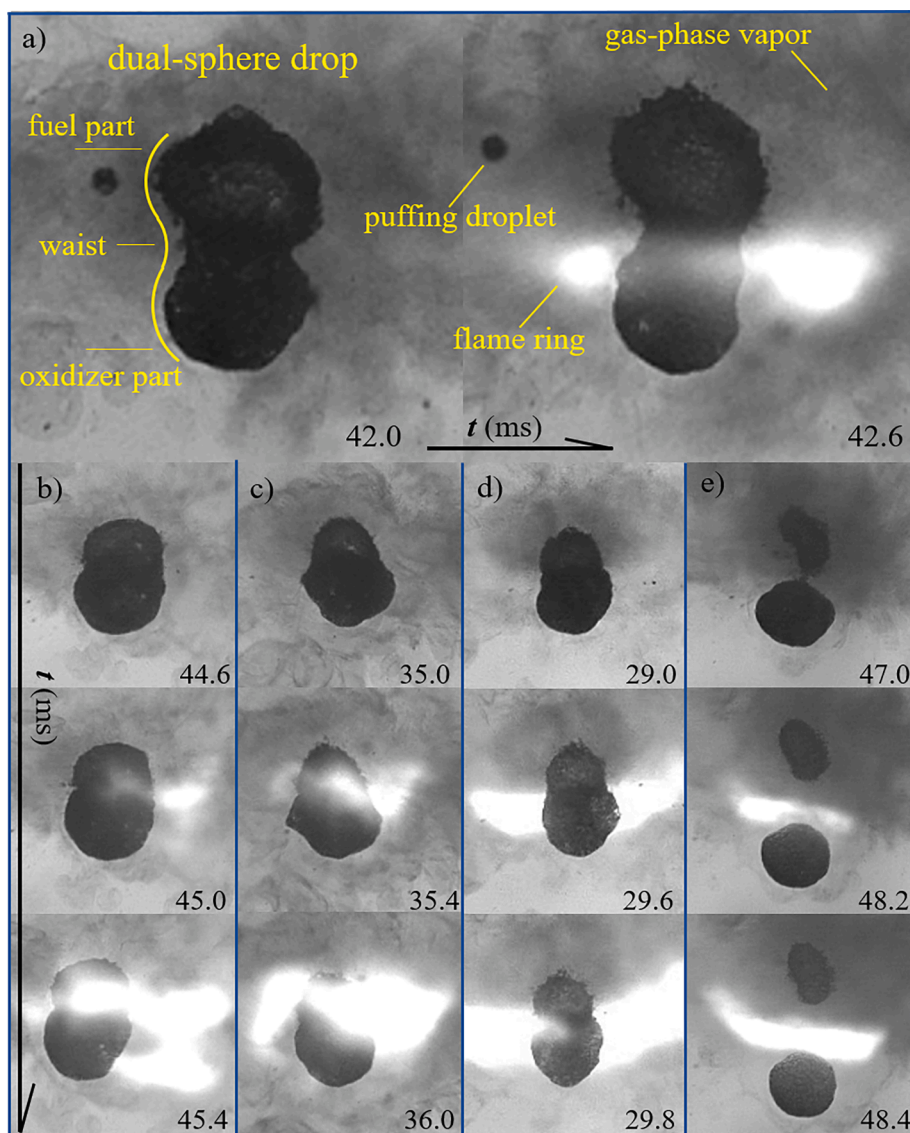
Fig. 11. Duel-sphere droplet and flame ring at various cases: a)$We = 41$, $\Delta = 1.75$; b) $We = 61$, $\Delta = 1.75$; c)$We = 31$, $\Delta = 1.35$; d)$We = 61$, $\Delta = 1.35$; and e) $We = 41$, $\Delta = 2.15$.

structure developing stage II, and then starts to increase at a moderate rate for a certain period, and then dramatically increases up all of a sudden. According to the experimental result, during the rapid swelling period, the droplet expands about 4 times in volume within 5.0 ms.

In addition, large-scale bubbles also can be directly recognized inside the droplet as indicated in Fig. 8b ~ 8e. The location and distribution pattern of bubbles are similar to that appeared in the biomass oil droplet when burning in the reactor [34]. In particular, for bubbles generated near the droplet surface they are so likely to break through the tensional constraint that the internal matters are puffing out, as observed at 39.0 ms in Fig. 8a. While for those formed at the droplet central zone, they are of great possibility to merge into larger bubbles. It is the generation of interior bubbles that is considered to cause droplet swelling.

Doubtlessly, the existence of bubbles signifies the formation of gas-phase species. As to the present pair of fuel and oxidizer, the gaseous species are possibly formed by two mechanisms: (1) the gas-producing reaction of H_2O_2 self-decomposition; (2) the flash vaporization of the superheated oxidizer mass inside the coalesced droplet. To identify the controlling process for the present case, the gas accumulation rates of both mechanisms are calculated.

As for the H_2O_2 self-decomposition, if considering the reaction rate

(from the previous experimental data [35]) for droplet swelling, one can find that it will take hundreds of times longer for the decomposition to generate a comparable volume of gaseous species at even elevated environmental temperatures.

As for the flash vaporization, a theoretical model [36] concerning the gasification of the inner liquid heated up by the surrounding hot liquid is applied herein. Assuming the circumstantial hot liquid has a higher boiling temperature than the inner heated liquid, this model can be expressed by

$$\frac{dR}{dt} = \left(\frac{3}{\pi}\right)^{1/2} \frac{\lambda}{L\rho_v} \frac{T_\infty - T_b}{(\alpha t)^{1/2}} \tag{3}$$

Integrating the above equation we have,

$$R_{bubble} = 2\lambda \left(\frac{3}{\pi\alpha}\right)^{1/2} \frac{T_\infty - T_b}{L\rho_v} t^{1/2} \tag{4}$$

where ρ_v is equilibrium vapor density at the boiling temperature, and T_∞ and T_b are the temperatures of the circumstantial hot liquid and the boiling temperature of the inner heated liquid respectively. In the present study, T_∞ was set as the boiling point of MEA, and T_b is represented
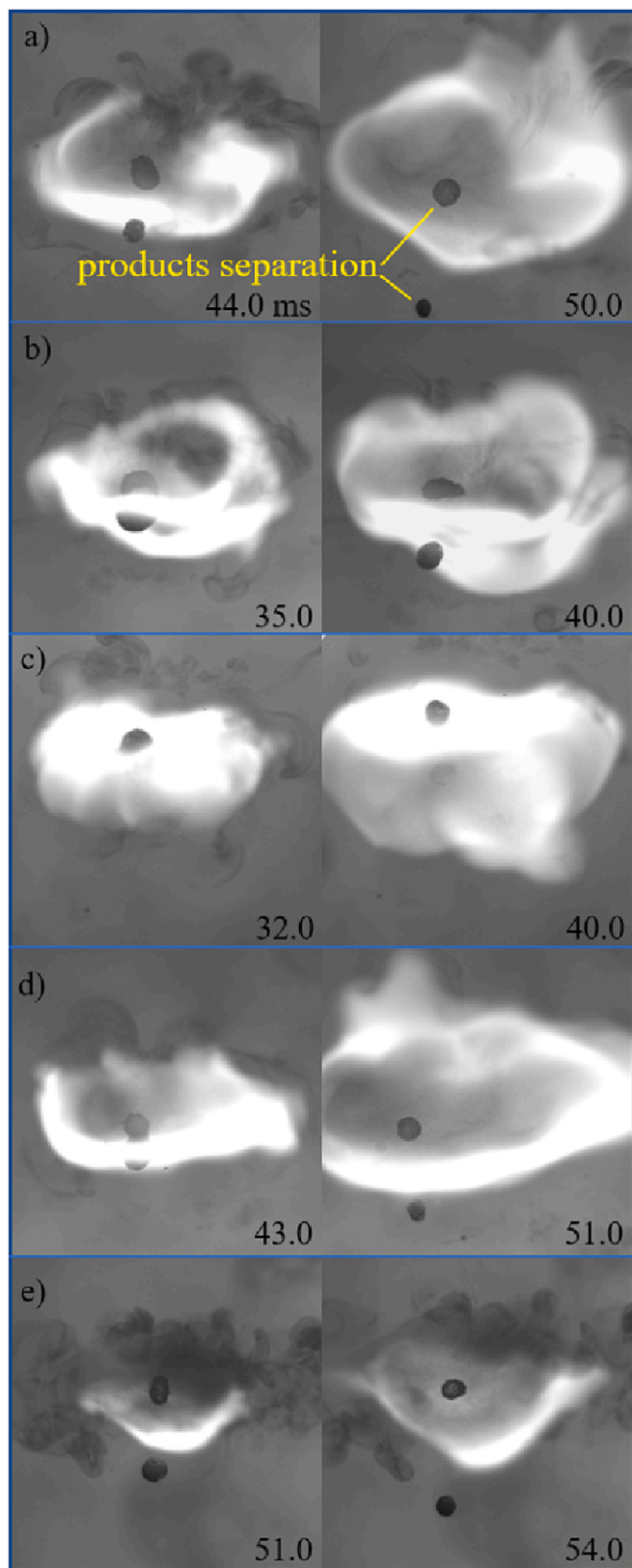
Fig. 12. Flame expansion at a) $We = 41$, $\Delta = 1.75$; b) $We = 61$, $\Delta = 1.75$; c) $We = 31$, $\Delta = 1.35$; d) $We = 61$, $\Delta = 1.35$; e) $We = 41$, $\Delta = 2.15$.

by the boiling point of H_2O_2. The term $T_\infty - T_b$ can be regarded as a measure of the level of superheating of the inner liquid.

As has been reported in [36], at the beginning of the vapor bubble generation inside the droplet, the surface tension and inertial force would predominate the process. Under the surface constraint and inertial drag, the bubbles expand at a moderate swelling rate, as indicated in Fig. 9. As the expansion continues, the input thermal energy balances out the required amount of heat for the bubbles to expand. The droplet interior is thereby filled up rapidly with gaseous species. This in turn leads to the dramatic growth of the bubbles which corresponds to the swelling of the droplet. In the present experiment, the volume of the measured droplet should equal the sum of the volumes of the internal inflating bubbles and the original droplet, so it gives

$$\left(\frac{R}{R_{og}}\right)^3 = \left(\frac{R_{bubble}}{R_{og}}\right)^3 + 1 \tag{5}$$

Substituting Eq. (4) into Eq. (5) and after some arrangement, one can get the explicit expression of droplet volume at different moments during the swelling as,

$$\left(\frac{R}{R_{og}}\right)^3 = \kappa t^{3/2} + 1 \tag{6}$$

where the factor $K = 7.47 \left[\frac{\lambda (T_\infty - T_b)}{\alpha^{1/2} L \rho_v R_{og}} \right]^3$.

Fig. 10 shows the normalized droplet volume with various collision Wes and Δs during pre-ignition. The periods that droplet volume first remains constant and then moderately expands, as in the representative case, emerge as well in all the other cases, signifying the prevalence of development of internal structure and the generation of bubbles inside the droplet. During the moderate expansion, droplet volume grows but is limited up to 1.2 times larger than the original value.

The rapid swelling stage emerges for also all the cases, and it is found starting earlier for larger Wes and smaller Δs as shown in the sub-figure in Fig. 10 where the starting moment of the rapid swelling is plotted with respect to We at various Δs. By comparison, the measured droplet volume is found to agree quite well with the prediction by Eq. (6). Since Eq. (6) is formulated based on the mechanism of rapid vapor accumulation, the coincidence between experimental and theoretical results in turn verifies the conclusion that the swelling is controlled by flash vaporization of the inner H_2O_2 liquid. The vapor trapped inside the bubbles could serve as the oxidizer when they puff out participating in the gas-phase ignition.

3.4. Flame initiation and propagation with double-bell-shaped droplet

Along with droplet swelling, the interfacial boundary, defined above, separating the distorted and undisturbed parts of the droplet keeps developing and becomes susceptible to breakdown. Once inner vapor puffs out from such area the droplet deforms into a double-bell shape with a waist connecting two superficially distinct parts as schematized in Fig. 11a. The undisturbed part of the double-bell droplet consists mainly of the non-reacting MEA fuel mixture, while the other swelling and deforming part contains largely the oxidizer mass undergoing violent exothermal reactions with $NaBH_4$. After being heated up, a large amount of thermal energy is transported outward from the reacting part and a noticeable amount of dark vapor is detected surrounding the droplet as indicated at 42.6 ms in Fig. 11a.

Once the flammable fuel vapor meets the hot gaseous oxidizer puffing out from the droplet, the ignition is triggered. Since the gaseous oxidizer species break out primarily from the waist area of the double-bell droplet, bright flame signifying the ignition first arises in a ring shape surrounding the droplet as shown in Fig. 11a., for all the representing collision cases shown in Fig. 11a ~ 11e, the ring-shaped flame structure manifest with no exception at the waist area. One interesting phenomenon is that for collision $\Delta = 2.15$ and $We = 41$ as in Fig. 11e, the
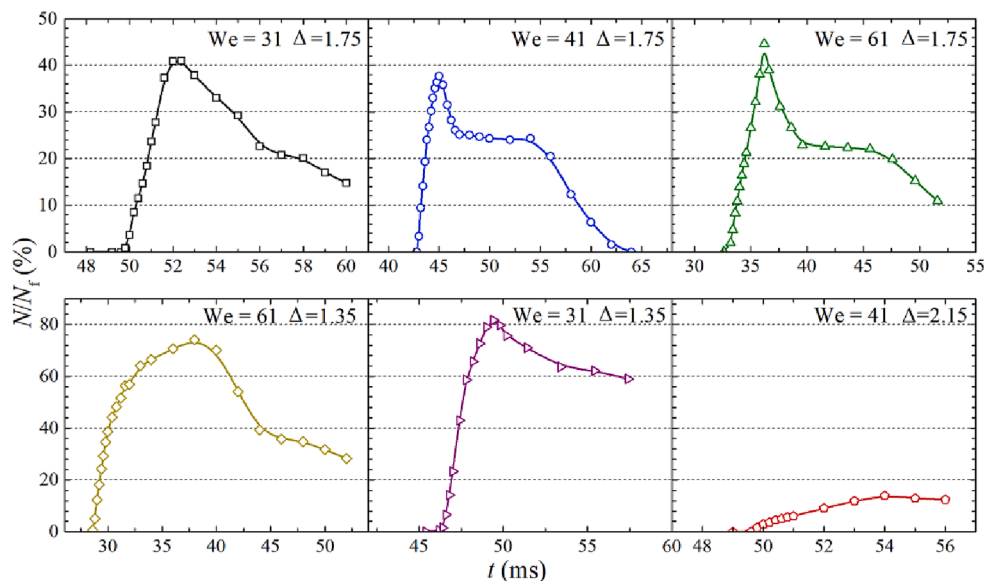
Fig. 13. The bright flame developments for cases at various *We*s and Δ s.

two parts of the double-bell droplet separate away from each other when ignition occurs. The underlying reason is that the large discrepancy in droplet size makes the inner smaller droplet reside mostly at the polar surface of the larger fuel droplet, so it is more likely to break up the surface constraint to separate away.

As time proceeds, the ring-shaped flame expands, enveloping the droplet, as shown in Fig. 12. The flame propagates at a rapid rate, consuming the combustible dark gaseous species such that the dark vapors have been replaced by the luminous flame. In course of the propagation of flame, the evaporation of the droplet is expedited. The gaseous fuel is continuously supplied to the flame zone to sustain the combustion. As shown in the second column in Fig. 12, the bright flame occupies mainly the fuel part of the droplet, while the other part has already flown away containing the non-flammable condensed-phase products.

As defined before, the bright flame in the shadow image is distinguished by the pixels with a gray-level G value larger than 200. By counting the pixels number, N, with $G \geq 200$, we obtain the measured projective area of the bright flame in the referenced frame that contains the total pixels of N_r. Fig. 13 shows the ratio of N/N_r at various *We*s and Δs. Note that N always maintains a minimum value of zero during the whole pre-ignition stages until the occurrence of the bright flame. Once ignition happens it starts to increase abruptly to its maximum level. During the dying-out period of the flame, the bright area shrinks rapidly as the gaseous fuel is depleted. While between the extinction and the peak of the flame, there exists a specific stage during which the flame maintains its area for a certain length of time. It is the period when the flame propagates, heating and vaporizing the fuel droplet to produce further the flammable gaseous species that in turn sustains the flame. As seen from the figure, in most cases the flame lasts in each case for more than ten milliseconds. While for the case of $We = 41$, Δ = 2.15, the flame area is much smaller because of the earlier separation of the two parts of the reacting double-bell droplet.

4. Concluding remarks

Hypergolic ignition by the binary collision of Monoethanolamine-NaBH$_4$-based fuel and H$_2$O$_2$ droplets has been experimentally examined with an emphasis on inter-mixing and heat transfer patterns during the pre-ignition stages and on the flame structures after ignition.

Five stages are phenomenally defined based on the characters of the droplet and flame. As to the collision stage, the fuel and oxidizer droplets

behave as if they were non-reactive ones. For the second stage, the deformed H$_2$O$_2$ droplet regained its spherical shape inside the MEA fuel mixture droplet. The restoration process is verified and driven by the interfacial tension between the oxidizer and fuel liquids. The interfacial-tension-driven mechanism was further theoretically verified by an *ad hoc* model based on linear stability analysis of droplet oscillation in a viscous liquid environment. During Stage III, large bubbles are observed nucleating and merging at the center of the droplet. A theoretical model balancing the thermal energy in to and out of the droplet was addressed to provide a quantitative interpretation of droplet swelling. The droplet expands first at a moderate rate, owing to the constraint from the surface tension and the drag of the droplet inertia. The increase rate in the volume of the bubbles is independent of collision-related parameters, such as *We*s and Δ s, as the controlling mechanism is only related to heat transportation. During the swelling, a double-bell-shaped droplet is formed consisting of one undisturbed fuel mixture part and the other reacting oxidizer part. When the ignition is triggered, a ring-shaped flame is captured surrounding the waist of the double-bell drop. Bright flame expands rapidly in subsequence, enveloping the droplets, and lasts for more than 10.0 ms.

A knowledge of inter-mixing inside the droplet during the pre-ignition period is essential to interpret the heat transfer pattern during the pre-ignition period. Details of the droplet structure turn out to be requisite to the following flame feature and its propagation. Therefore, a uniform experimental and theoretical frame quantifying the characteristics during the ignition process for a wide range of groups of fuel and oxidizers must be of great significance and merit future concerns.

CRediT authorship contribution statement

Dawei Zhang: Conceptualization, Methodology, Formal analysis. **Dehai Yu:** Formal analysis, Investigation. **Peng Zhang:** Supervision. **Xuejun Fan:** Funding acquisition.

Declaration of Competing Interest

The authors declare that they have no known competing financial interests or personal relationships that could have appeared to influence the work reported in this paper.

Data availability

Data will be made available on request.

References

[1] Fletcher EA, Morrell G. Ignition in liquid propellant rocket engines. In: Ducerme MGJ, Lefebvre AH, editors. Progress in Combustion Science and Technology. New York: Pergamon; 1960. p. 183–215.

[2] Eric RJM, Hurlbert A. Propellant ignition and flame propagation. In: Yang V, Habiballah M, Hulka J, Popp M, editors. Liquid Rocket Thrust Chambers: Aspects of Modeling, Analysis, and Design. Virginia: American Institute of Aeronautics and Astronautics Inc; 2004. p. 421–30.

[3] Sutton GP, Biblarz O. Rocket propulsion elements. 8th ed. New Jersey: John Wiley & Sons; 2010.

[4] SM. Davis, N. Yilmaz. Advances in Hypergolic Propellants: Ignition, Hydrazine, and Hydrogen Peroxide Research. Adv Aerosp Eng. 2014; 1:1-9. https://doi. org/ 10.1155/j.aae.2014.729313.

[5] Kilpatrick M, Baker LL. A study of fast reactions in fuel-oxidant systems: Anhydrous hydrazine with 100 percent nitric acid. Symp (Int) Combust 1955;5(1):196–205.

[6] S. Wang, ST. Thynell, A. Chowdhury. Experimental study on hypergolic interaction between N, N, N′, N′-tetramethylethylenediamine and nitric acid. Energ Fuel. 2010; 24:5320-5330. https://doi. org/10.1021/j.ef.2010.100593s.

[7] JD. Dennis, SF. Son, TL. Pourpoint. Critical ignition criteria for monomethylhydrazine and red fuming nitric acid in an impinging jet apparatus. Atlanta: 48th AIAA/ASME/SAE/ASEE Joint Propulsion Conference; 2012, p. 2012-4325. 10.2514/6.2012-4325.

[8] S. Wang, TL. Thynell. An experimental study on the hypergolic interaction between monomethylhydrazine and nitric acid. Combust Flame. 2012; 159:438-447. https://doi. org/10.1016/j.combustflame.2011.07009.

[9] Dambach EM, Solomon Y, Heister SD, Pourpoint TL. Investigation into the Hypergolic Ignition Process Initiated by Low Weber Number Collisions. J Propul Power 2013;29:331–8. https://doi.org/10.2514/1.B34627.

[10] Jiang YJ, Umemura A, Law CK. An Experimental Investigation on the Collision Behavior of Hydrocarbon Droplets. J Fluid Mech 1992;234:171–90. https://doi.org/10.1017/S0022112092000740.

[11] Qian J, Law CK. Regimes of coalescence and separation in droplet collision. J Fluid Mech 1997;331:59–80. https://doi.org/10.1017/S0022112096003722.

[12] JD. Dennis, TL. Pourpoint, SF. Son. Ignition of Gelled Monomethylhydrazine and Red Fuming Nitric Acid in an Impinging Jet Apparatus. California: 47th AIAA/ ASME/SAE/ASEE Joint Propulsion Conference; 2011, e5706. 10.2514/6.2011-5706.

[13] TL. Connell, GA. Risha, RA. Yetter, B. Natan. Effect of Fuel Type on Hypergolic Ignition of Hydrogen Peroxide with Gelled Hydrocarbon Fuel. Cleveland: 50th AIAA/ASME/SAE/ASEE Joint Propulsion Conference; 2014, e3470. 10.2514/ 6.2014-3470.

[14] Florczuk W, Rarata G. Assessment of various fuel additives for reliable hypergolic ignition with 98%+ HTP. Jerusalem: 66th International Astronautical Congress; 2015. p. 1–8.

[15] B. Jyoti, MS. Naseem, SW. Baek. Hypergolicity and ignition delay study of pure and energized ethanol gel fuel with hydrogen peroxide. Combust Flame. 2017; 176: 318-325. https://doi. org/10.1016/j.combustflame.2017.05007.

[16] BVS. Jyoti, MS. Naseem, SW. Baek, HJ. Lee, SJ. Cho. Hypergolicity and ignition delay study of gelled ethanolamine fuel. Combust Flame. 2017; 183:102-112. https://doi. org/10.1016/j.combustflame.2016.11018.

[17] Law CK. Combustion physics. London: Cambridge University Press; 2010.

[18] D. Zhang, D. Yu, P. Zhang, Y. Yuan, L. Yue, T. Zhang, X. Fan. Hypergolic ignition modulated by head-on collision, intermixing and convective cooling of binary droplets with varying sizes. Int J Heat Mass Tran. 2019; 139:475-481. https://doi.org//10.1016/j.ijheatmasstransfer.2019.05040.

[19] Zhang D, Zhang P, Yuan Y, Zhang T. Hypergolic ignition by head-on collision of N, N,N′,N′ −tetramethylethylenediamine and white fuming nitric acid droplets. Combust Flame 2016;173:276–87.

[20] Zhang D, He C, Zhang P, Tang C. Mass intermingment and hypergolic ignition of TMEDA and WFNA droplets by off-center collision. Combustion Flame 2018;197: 276–89.

[21] Tang C, Zhao J, Zhang P, Law CK, Huang Z. Dynamics of Internal Jets in the Merging of Two Droplets of Unequal Sizes. J Fluid Mech 2016;795:671–89.

[22] C. Tang, P. Zhang, C.K. Law, Bouncing, coalescence, and separation in head-on collision of unequal-size droplets, Phys Fluids. 2012; 24:022101. 10.1063/ 1.3679165.

[23] Ashgriz N, Poo JY. Coalescence and separation in binary collisions of liquid drops. J Fluid Mech 1990;221:183–204. https://doi.org/10.1017/S0022112090003536.

[24] Ak M, Ulas A, Sümer B, Yazıcı B, Yıldırım C, Gönc L, et al. An experimental study on the hypergolic ignition of hydrogen peroxide and ethanolamine. Fuel 2011;90: 395–8. https://doi.org/10.1016/j.fuel.2010.07048.

[25] Jyoti BVS, Baek SW. Rheological characterization of ethanolamine gel propellants. J Energ Mater 2016;34(3):260–78.

[26] B. Melof, M Grubelich. Investigation of hypergolic fuels with hydrogen peroxide. Salt Lake City: 37th Joint Propulsion Conference and Exhibit; 2001, e3837. 10.2514/6.2001-3837.

[27] M. Ventura, E. Wernimont, S. Heister, S. Yuan. Rocket Grade Hydrogen Peroxide for use in Propulsion and Power Devices-Historical Discussion of Hazards. Cincinnati: 43th AIAA/ASME/SAE/ASEE Joint Propulsion Conference; 2001, p. 2007-5468. 10.2514/6.2007-5468.

[28] Gohardani AS, Stanojev J, Demairé A, Anflo K, Persson M, Wingborg N, et al. Green space propulsion: Opportunities and prospects. Prog Aerosp Sci 2014;71:128–49. https://doi.org/10.1016/j.paerosci.2014.08001.

[29] Connell TL, Risha GA, Yetter RA, Natan B. Ignition of Hydrogen Peroxide with Gel Hydrocarbon Fuels. J Propul Power 2018;34(1):170–81.

[30] R. Mahakali, F. Kuipers, A. Yan, W. Anderson, T. Pourpoint. Development of reduced toxicity hypergolic propellants. California: 47th AIAA/ASME/SAE/ASEE Joint Propulsion Conference; 2001, p. 2011-5631. 10.2514/6.2011-5631.

[31] Kang H, Won J, Baek SW, Kwon S. Autoignition and combustion characteristics of sodium borohydride-based non-toxic hypergolic fuel droplet at elevated temperatures. Combust Flame 2017;181:149–56. https://doi.org/10.1016/j.combustflame.2017.03.021.

[32] Miller C, Scriven L. The oscillations of a fluid droplet immersed in another fluid. J Fluid Mech 1968;32:417–35. https://doi.org/10.1017/S0022112068000832.

[33] Demond AH, Lindner A. Estimation of interfacial tension between organic liquids and water. Environ Sci Tech 1993;27:2318–31. https://doi.org/10.1021/es00048a004.

[34] Wornat MJ, Porter BG, Yang N. Single droplet combustion of biomass pyrolysis oils. Energ Fuels 1994;8:1131–42. https://doi.org/10.1021/ef00047a018.

[35] Lin C, Smith F, Ichikawa N, Baba T, Itow M. Decomposition of hydrogen peroxide in aqueous solutions at elevated temperatures. Int J Chem Kinet 1991;23:971–87. https://doi.org/10.1002/kin.550231103.

[36] Prosperetti A, Plesset M. Vapor-bubble growth in a superheated liquid. J Fluid Mech 1978;85:349–68. https://doi.org/10.1017/S0022112078000671.